PHYSICAL REVIEW B **92**, 100301(R) (2015)

Observation of shape-preserving accelerating underwater acoustic beams

Uri Bar-Ziv,[1,2] Aharon Postan,[2] and Mordechai Segev[1]
[1]*Technion–Israel Institute of Technology, Technion City 3200003, Haifa, Israel*
[2]*Rafael Advanced Defense Systems LTD, P.O. Box 2250, Haifa 3102102, Israel*
(Received 12 February 2015; revised manuscript received 2 August 2015; published 1 September 2015)

We present the experimental generation and observation of an underwater acoustic accelerating beam. The beam was generated by phase modulating a single projector using a tailored acoustic phase mask. The beam is propagating for a range in excess of 800 wavelengths, which are about six Rayleigh lengths, while preserving its shape and transversely accelerating. Such beams have promising applications in the fields of sonar, hydrography, and medical ultrasound and can provide new means to study nonlinear interaction of acoustic beams.

DOI: 10.1103/PhysRevB.92.100301 PACS number(s): 42.25.−p

The accelerating shape-preserving solution of the potential-free Schrödinger equation was introduced in 1979 [1], identifying the Airy wave function that accelerates parabolically. However, the Airy function is not square integrable, hence it cannot represent a probability density. The idea of shape-preserving accelerating wave packets was therefore abandoned for almost three decades, until it was introduced into optics, based on the mathematical equivalence of the Schrödinger equation and the paraxial wave equation [2,3]. It was then shown that truncation of the Airy wave form yields shape-preserving acceleration to within a finite range. Since then, the field has attracted significant attention owing to promising applications such as micromanipulation of particles [4], generation of curved plasma channels in the air [5], micromachining of curved surfaces [6], light sheet microscopy [7], and three-dimensional fluorescent imaging [8]. Subsequent research led to finding a family of accelerating shape-preserving solutions of the $(2+1)D$ paraxial wave equation [9–11]. The concept was generalized to finite-power nonbroadening accelerating beams that can propagate on any (arbitrary) convex trajectory [12–14]. A significant step was subsequently made by the prediction [15] and experimental demonstration [16] of nondiffracting accelerating solutions of the full Maxwell equations. Light beams described by such solutions can bend to almost 180° [15], unlike the paraxial case where the Airy beam deforms beyond paraxial angles. Other solutions and generalizations followed soon thereafter [17–20]. These "self-bending beams" were all based on linear wave diffraction physics. However, nondiffracting accelerating beams were also studied in nonlinear media, in the paraxial [21,22] and nonparaxial regimes [23,24]. Such beams were demonstrated with quadratic nonlinearity, exhibiting joint acceleration of the coupled harmonics, but with asynchronous intensity pattern [25]. Interestingly, all types of accelerating beams share the property of self-healing: they self-reconstruct during propagation in the presence of a disturbance. This is of importance when such beams propagate in inhomogeneous media [26]. Moreover, new solutions were obtained recently [27,28], presenting loss-proof self-accelerating beams, with applications for manipulating microparticles in lossy fluids [27].

Importantly, shape-preserving accelerating wave packets were also studied beyond optics, for example with electron beams [29], Bose-Einstein condensates [30], and Dirac fermions [31]. In a different domain, nondiffracting acoustic Bessel beams were demonstrated more than two decades ago [32], but, just recently, pioneering work demonstrated acoustic accelerating beams in gas (air) [33]. There, an array of speakers with specific phase distribution was used to launch acoustic bottle beams and Bezier beams. However, many applications of acoustics are in liquids. Examples range from ultrasound imaging and ultrasonic therapy in the medical arena, sonar, hydrography, and underwater communication, to ultrasonic microscopy where the specimen is immersed in liquid to guarantee good coupling of the acoustic wave. Importantly, it was recently suggested that acoustic half-Bessel beams could be used for microparticle transport in liquids [34]. Interestingly, under some conditions, the propagation of acoustic beams becomes nonlinear [35–38], which could be used to generate nonlinear accelerating acoustic beams, presenting even richer phenomenology than their optical counterparts. Moreover, adding gas microbubbles to liquids introduces a new kind of acoustic nonlinearities [39] that can support nonlinear accelerating wave packets of fundamentally new types. It was recently proposed that a piston transducer with a corrugated face, specifically tailored, could generate acoustic Airy beams in liquids [40]. However, to this day, not a single experiment was ever reported on acoustic accelerating beams in liquids.

Here, we do just that, using a novel underwater acoustic setup, and demonstrate an acoustic accelerating beam in a liquid: an underwater acoustic shape-preserving accelerating beam. We emphasize that the experimental system for shaping the launch acoustic beam in a liquid is very different than shaping the acoustic wave packet in gas. Namely, liquids are generally characterized by acoustic impedance orders of magnitude higher than of gas. In fact, the acoustic impedance in liquid is close to the impedance of some solids. Consequently, we use a phase mask (made from solid material) in transmission mode, which takes advantage of the fact that the transmission is efficient (as the impedance mismatch between the mask and the liquid is small).

Since this Rapid Communication deals with underwater acoustic waves, introduction on this subject is useful. Although acoustic phenomena in fluids often involve nonlinear processes, it is common to describe low-amplitude acoustic waves in fluids in the linear limit by the scalar wave equation. The equation is derived by linearization of the Navier-Stokes and thermodynamical relations [41]. Consequently, directional acoustic beams are described by the paraxial wave equation

familiar from electromagnetism, for which the Airy beams are the unique shape-preserving accelerating beam solutions in one transverse dimension.

We begin with the wave equation that describes the propagation of time-harmonic paraxial beams:

$$\left(2ik\partial_z + \partial_x^2\right)\psi = 0. \tag{1}$$

Here, k is the wave number, z is the paraxial propagation direction, x is a transverse coordinate, and $\psi = \phi e^{-ikz}$ is the slowly varying envelope of the wave function $\phi(x,z)$. The shape-preserving accelerating solution of Eq. (1) is the Airy wave packet [1,3], which at the launch plane $z = 0$ is

$$\psi(x,z=0) = \psi_0 \mathrm{Ai}[(4ak^2)^{1/3}x], \tag{2}$$

where Ai designates the Airy function, a is a real valued acceleration rate parameter, and ψ_0 is an arbitrary complex amplitude. This solution is propagating on the parabolic trajectory $x = az^2$. In our work, practical considerations led us to choose to excite the accelerating wave packet by a phase-only initial condition. Our setup follows [12,42], where the accelerating beam was launched by passing a plane wave through the one-dimensional phase distribution imposed by a spatial light modulator, and the accelerating beam forms after some distance within which the pattern experienced Fresnel diffraction. For launching an Airy beam, the appropriate phase structure at the launch plane is [42]

$$\varphi_{\mathrm{acc}}(x) = \begin{cases} -(4/3)k\sqrt{a}(-x)^{3/2}, & x < 0 \\ 0, & x \geqslant 0 \end{cases}. \tag{3}$$

Using this expression at $z = 0$ with constant amplitude, and following the procedure in [12] by applying the stationary phase approximation in the Fresnel integral, the field $\psi(x, z \geqslant z_f)$ after some distance z_f can be approximated as

$$\psi = \begin{cases} \sum_{\pm} B_{\pm}\mathrm{Ai}[(-2k/a)^{2/3}(A_{\pm}/z - \sqrt{aA_{\pm}})^2], & x < az^2 \\ 2\pi(-4a/k)^{1/3}e^{ik(2a^2z^3/3)}\mathrm{Ai}(0)z, & x = az^2 \\ 0, & x > az^2 \end{cases} \tag{4}$$

with

$$\begin{aligned} A_{\pm} &= -x + 2az^2(1 \pm \sqrt{1 - x/az^2}), \\ B_{\pm} &= 2\pi(-4/k\sqrt{a})^{1/3}\sqrt{A_{\pm}}e^{ik[(x+A_{\pm})^2/2z - 4\sqrt{a}A_{\pm}^{3/2}/3]}. \end{aligned} \tag{5}$$

We find that specifying $x = az^2$ zeroes the argument of the Airy function, manifesting the parabolic trajectory of the peak amplitude.

Our experiments are carried out at the Rafael underwater test tank whose dimensions are L × W × D = 20 × 10 × 10 m, where D is the depth. Our goal is to generate a beam that would display acceleration up to the maximum range possible in our water tank, which, for practical reasons is up to 15 m. The frequency is chosen to be 200 kHz, which implies an acoustic wavelength of approximately 7.5 mm and negligible loss (over the length scales involved) in water. To support 15 m of propagation of a shape-invariant beam, the aperture required is ∼1 m. This poses a practical difficulty: the acoustic projector acts as a point source and delivers a spherically spreading field, whereas the desired shape that would pass through a phase mask should be a plane wave. Since we cannot position the acoustic projector far away from the phase mask (because this would considerably reduce the propagation distance available in the tank), the solution is to design the phase mask to also compensate for the phase variation of the spherical wave front. Hence, the phase encoded must both transform the diverging spherical wave into an approximate plane wave, and at the same time encode the desired phase distribution of Eq. (3). The aperture of the acoustic phase mask is extended in the transverse y coordinate, such that the acceleration dynamics appears in the x-z plane while the beam acts as a plane wave in y. These considerations result in

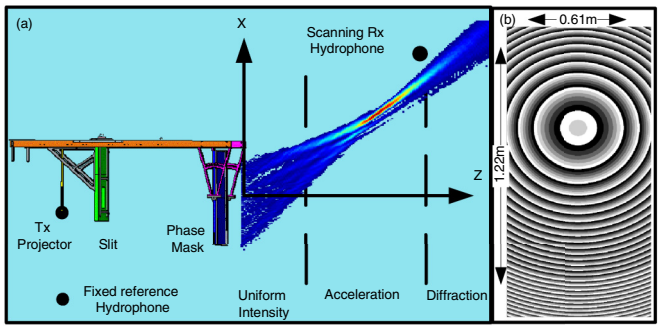

FIG. 1. (Color online) (a) Experimental setup. The source is a spherical acoustic projector that emits a diverging spherical wave front at a prescribed frequency. The wave is propagating through a slit (made from acoustic absorbing tile) designed to minimize interference from waves escaping the finite-sized phase mask. The wave is then passing through a phase mask that encodes a combination of a quadratic phase (converting the spherical wave front into a semiplanar one), and a one-dimensional phase increasing with distance to power (3/2). This sets the initial condition for the generation of the accelerating beam. The detection is carried out with a receive hydrophone, where the acoustic field is scanned along the x-z coordinates. A fixed reference hydrophone, positioned next to the projector, monitors the actual acoustic intensity output. (b) The phase encoded on the phase mask.

$$\varphi(x,y) = \mathrm{mod}_{2\pi}[k(x^2 + y^2)/2f + \varphi_{\mathrm{acc}}(x - L/2)] \tag{6}$$

at the launch plane, where f is the distance from acoustic projector to the phase mask (within which the wave front is of a spherical wave), and L is the aperture in the x direction.

We now describe our setup [Fig. 1(a)]. The phase mask is made from a plate of Rexolite-1422 plastic (cross-linked polystyrene), which has good acoustic impedance matching to water (acoustic impedance of 2.48 MRayl compared to 1.5 MRayl of water), negligible absorption, and a refractive index of $n \simeq 0.63$(datasheet sound velocity of 93 000 in./s which are roughly 2362 m/s), while the sound velocity in water during the experiment was ∼1492 m/s). The dimensions of the plate are 1.22 × 0.61 m (x-y). The phase is encoded on the plate by machining the plate to the proper thickness. The phase distribution [Eq. (3)] giving rise to acceleration varies between zero and $-16 \times 2\pi$ rad. Since the phase has significance only up to modulo (2π), we fold the phase as in a Fresnel lens. The surface of the mask is made of contours such that the mask is flat between contours. Each contour is assigned with one of six thickness values, corresponding to $(0°, 60° \ldots, 300°)$ phase levels, and parameters $a = 0.005\ \mathrm{m}^{-1}$, $f = 2$ m. Figure 1(b)

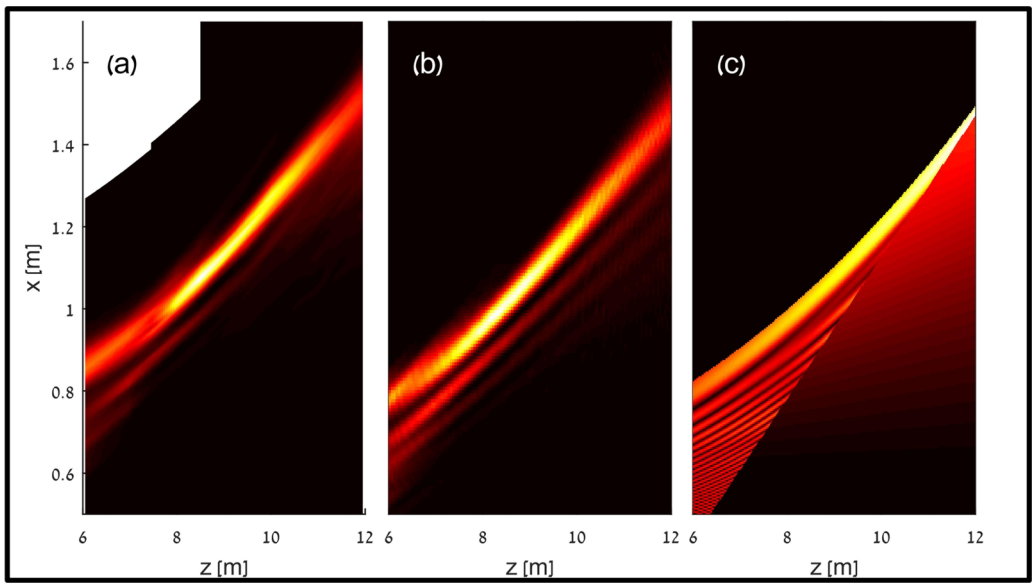

FIG. 2. (Color online) (a) Experimentally measured intensity (normalized) of the self-accelerating beam. (b) Numerical simulation of the same scenario. (c) The approximate closed-form expression given by Eq. (4), for the same beam acceleration parameter and aperture. The blank region in (a) indicates regions where no measurements were taken.

displays the phase mapped to the surface of the mask. The acoustic source (Neptune Sonar D-140 spherical projector powered by a Brüel & Kjær 2713 power amplifier), is carefully positioned along the acoustic axis, at $f = 2$ m behind the phase mask. A plate of acoustic absorbing tile (Precision Acoustics Apltile SF5048) is used to eliminate interference effects from waves bypassing the phase mask. The absorbing plate positioned 0.5 m from the projector, between the projector and the phase mask, has a slit cut to appropriate shape and dimensions. The entire system is held together by a fixture, and suspended by straps in the water tank at approximately 5 m depth. An underwater electronic level is used together with adjustment screws to correct the attitude of the fixture. For calibration purposes, we position a reference hydrophone (Reson TC-4034) perpendicular to the acoustic axis at 5 m depth, 3.1 m away from the projector, such that it is directly exposed to sound from the projector. The receive hydrophone (Reson TC-4034) is held by a rod set from an overwater translatable bridge. A measure tape is attached to the rod, and the rod is shifted up and down to measure along the x coordinate. Similarly, the bridge is translated along the tank for measurement at different propagation planes z. The signals are amplified by Brüel & Kjær 2610 measuring amplifiers, and captured by a NI-DAQ 6366 digitizer.

During the experiment, the acoustic field is scanned manually over 1000 x-z grid points in intervals of ∼50 cm along the z direction, and smaller intervals of ∼1 cm in the x direction. At each grid point, the measurement is first calibrated by launching a sequence of short acoustic pulses (5–10 cycles), which is transmitted through the system and detected, where accurate calibration of the z coordinate is obtained by measuring the time delay and geometry. Following calibration, we generate the Airy beam by launching a sequence of long pulses (200–400 cycles, bandwidth of approximately 0.5–1 kHz), which are sufficiently long to allow for (temporal) transients to decay such that the propagating wave acts as a pseudocontinuous wave, and sufficiently short to separate unwanted echoes from the tank's boundaries. The acoustic intensity at each grid point is found by envelope detection of the stable portion of the long pulse, and averaging it over time and over the pulse sequence. The value of the intensity is normalized by the value obtained from the reference hydrophone, and corrected by hydrophone sensitivities, system gain, etc.

To visualize the acoustic beam at the various grid points, we first analyze each z slice of the grid to detect the location of the global maximum. With the position of the maximum in each propagation plane, we infer the beam trajectory, and interpolate along the curved coordinates of the trajectory. The results are shown in Fig. 2(a). The beam follows a parabolic trajectory and maintains its shape along the entire propagation length in the water tank. This experimental result is in good agreement with simulations [Fig. 2(b)] obtained by a beam propagation code simulating the system, including the effects of the spherical projector, slit, and phase mask. The beam's properties are also captured qualitatively by the approximate expression given by Eq. (4), as depicted in Fig. 2(c).

We now analyze the results quantitatively. First, we examine the beam's trajectory and fit the transverse location (in x) of the peak intensity of the beam in each propagation plane z, to a polynomial curve in the x-z plane. The best fit is shown in Fig. 3(a), and yields $x = 0.0062z^2 + 0.0021z + L/2$ (x, z in meters) where $L/2 = 0.3$ m is the displacement between the acoustic axis and the upper edge of the mask. Attempting the next order (cubic) polynomial fit to the measurements results in a negligible coefficient (-2×10^{-6}) for the cubic power, which indicates that the beam indeed curves as a parabola. The acceleration parameter obtained is 0.0062 m^{-1}, which is 20% higher than designed for. A possible explanation is that the sound velocity within the phase mask is 7% higher than the datasheet figure. The small linear dependence (in the polynomial fit) can be attributed to slight misleveling of

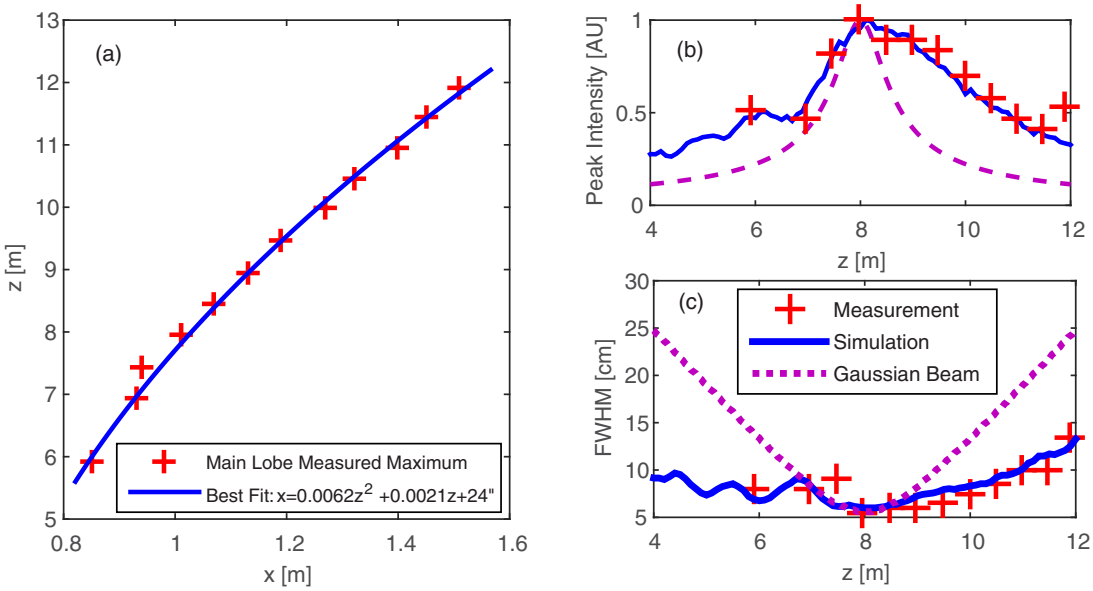

FIG. 3. (Color online) (a) Measured position of the peak of the main lobe in the x-z plane (red crosses) and best fit (blue). (b) Position of the (normalized) peak intensity of the main lobe as function of z, experimentally measured (red crosses), simulated (blue), and simulated evolution of the peak of a Gaussian Beam with identical waist width and z position (dashed purple). (c) Measured FWHM of the main lobe (red crosses) vs. simulation (blue) and a Gaussian beam as in (b) (dotted purple).

the system and is equivalent to $\sim 0.1^\circ$. Next, we examine the peak intensity of the beam as measured at each propagation plane, shown in Fig. 3(b). Along the entire propagation length, the peak intensity of the accelerating Airy beam decays to no less than 42% of its peak value. For comparison, we simulate the propagation of a Gaussian beam of the same full width at half maximum (FWHM) as the main lobe of the Airy beam. We position the waist of the simulated Gaussian beam at the global maximum of the intensity of our Airy beam (occurring in $z = 8$ m). The comparison reveals that the Gaussian beam experiences considerably more diffraction broadening, as evidenced by the reduction to 13% in its peak intensity [at 11.5 m distance in Fig. 3(b)]. In Fig. 3(c), we plot the FWHM of the main lobe of our beam as measured at each propagation plane, alongside with the FWHM of the Gaussian beam. Figure 3(c) further highlights the fact that the acoustic Airy beam experiences less diffraction broadening than a Gaussian beam. The Airy beam is only weakly broadening, exhibiting width variations of less than 8 cm, as compared to the 20 cm width broadening of the equivalent Gaussian beam. In other words, the acoustic Airy beam maintains a FWHM of 7–18 wavelengths along a propagation distance which is in excess of 800 wavelengths, which are over six Rayleigh lengths.

We conclude by discussing our results and ideas for future research. The full aperture in our setup was quite small (160 wavelengths), compared to typical setups available in optics (for example, in [12] the aperture, including the spatial light modulator and all lenses, was 20 000 wavelengths wide). This poses a major difficulty in launching the appropriate acoustic Airy beam. Furthermore, in our setting the distance between the acoustic source and the phase mask is similar to the extent of the aperture, which means that our incident wave was a spherical wave (rather than a pseudo plane wave in typical optical systems). These limitations, although they may seem practical, are actually intrinsic to underwater acoustics. Namely, launching underwater acoustic beams for distances of tens of meters sets a limit on the highest frequency that can be used, due to loss. Thus, the wavelength we used (7.5 mm) is roughly the shortest that can be used for our propagation distances. Nonetheless, in spite of these intrinsic limitations, our experiments are still able to demonstrate unequivocally an acoustic accelerating beam in a liquid. The beam maintains a narrow 7–10 wavelengths width along a significant propagation length, while exhibiting a parabolic trajectory. This remarkable feature suggests a means for conducting new experiments of nonlinear acoustics, specifically noncollinear interaction of acoustic beams for three-wave mixing and nonlinear frequency generation. Moreover, adding gas microbubbles to the liquid gives rise to a very large nonlinearity, acting in several different forms [39]. In some limit, the nonlinearity is similar to the quadratic nonlinearites in noncentrosymmetric dielectric media, which supports accelerating beams where the first and second harmonics accelerate locked to one another [21,25]. In another regime, the bubbles display different acoustic nonlinearities which have never been explored in the context of accelerating wave packets. Thus, our experiments pave the way for further research on acoustic accelerating wave packets in liquids, be they in water tanks or in biological tissues. Certainly, acoustic accelerating beams have promising applications in underwater and hydrographic acoustics, for example for detection and imaging of objects buried under the seabed. This can be assisted by the beam's ability to self heal and its characteristic asymmetric illumination/ isonification pattern that eliminates side lobes at one side of the beam. In biology and colloidal science, such beams facilitate the transport of microparticles along curved trajectories in liquids that are opaque to laser

light where optical manipulation (in the spirit of [27,28,43]) is not possible.

Note added. Recently, we learned about a related work on accelerating beams in liquid (see Ref. [44]). That paper demonstrated the propagation dynamics of surface gravity water waves, having an Airy function envelope, whereas our paper demonstrates accelerating underwater acoustic beams.

[1] M. V. Berry and N. Balazs, Am. J. Phys. **47**, 264 (1979).
[2] G. A. Siviloglou, J. Broky, A. Dogariu, and D. N. Christodoulides, Phys. Rev. Lett. **99**, 213901 (2007).
[3] G. A. Siviloglou and D. N. Christodoulides, Opt. Lett. **32**, 979 (2007).
[4] J. Baumgartl, M. Mazilu, and K. Dholakia, Nat. Photonics **2**, 675 (2008).
[5] P. Polynkin, M. Kolesik, J. Moloney, G. A. Siviloglou, and D. N. Christodoulides, Science **324**, 229 (2009).
[6] A. Mathis, F. Courvoisier, L. Froehly, L. Furfaro, M. Jacquot, P.-A. Lacourt, and J. M. Dudley, Appl. Phys. Lett. **101**, 071110 (2012).
[7] T. Vettenburg, H. I. Dalgarno, J. Nylk, C. Coll-Lladó, D. E. Ferrier, T. Čižmár, F. J. Gunn-Moore, and K. Dholakia, Nat. Methods **11**, 541 (2014).
[8] S. Jia, J. C. Vaughan, and X. Zhuang, Nat. Photonics **8**, 302 (2014).
[9] M. A. Bandres, Opt. Lett. **33**, 1678 (2008).
[10] J. A. Davis, M. J. Mitry, M. A. Bandres, and D. M. Cottrell, Opt. Express **16**, 12866 (2008).
[11] M. A. Bandres, Opt. Lett. **34**, 3791 (2009).
[12] E. Greenfield, M. Segev, W. Walasik, and O. Raz, Phys. Rev. Lett. **106**, 213902 (2011).
[13] L. Froehly, F. Courvoisier, A. Mathis, M. Jacquot, L. Furfaro, R. Giust, P. Lacourt, and J. Dudley, Opt. Express **19**, 16455 (2011).
[14] J. Zhao, P. Zhang, D. Deng, J. Liu, Y. Gao, I. D. Chremmos, N. K. Efremidis, D. N. Christodoulides, and Z. Chen, Opt. Lett. **38**, 498 (2013).
[15] I. Kaminer, R. Bekenstein, J. Nemirovsky, and M. Segev, Phys. Rev. Lett. **108**, 163901 (2012).
[16] F. Courvoisier, A. Mathis, L. Froehly, R. Giust, L. Furfaro, P.-A. Lacourt, M. Jacquot, and J. M. Dudley, Opt. Lett. **37**, 1736 (2012).
[17] P. Zhang, Y. Hu, T. Li, D. Cannan, X. Yin, R. Morandotti, Z. Chen, and X. Zhang, Phys. Rev. Lett. **109**, 193901 (2012).
[18] P. Aleahmad, M.-A. Miri, M. S. Mills, I. Kaminer, M. Segev, and D. N. Christodoulides, Phys. Rev. Lett. **109**, 203902 (2012).
[19] M. A. Bandres, M. A. Alonso, I. Kaminer, and M. Segev, Opt. Express **21**, 13917 (2013).
[20] M. A. Bandres, I. Kaminer, M. Mills, B. Rodríguez-Lara, E. Greenfield, M. Segev, and D. N. Christodoulides, Opt. Photonics News **24**, 30 (2013).
[21] I. Kaminer, M. Segev, and D. N. Christodoulides, Phys. Rev. Lett. **106**, 213903 (2011).
[22] P. Panagiotopoulos, D. Abdollahpour, A. Lotti, A. Couairon, D. Faccio, D. Papazoglou, and S. Tzortzakis, Phys. Rev. A **86**, 013842 (2012).
[23] P. Zhang, Y. Hu, D. Cannan, A. Salandrino, T. Li, R. Morandotti, X. Zhang, and Z. Chen, Opt. Lett. **37**, 2820 (2012).
[24] I. Kaminer, J. Nemirovsky, and M. Segev, Opt. Express **20**, 18827 (2012).
[25] I. Dolev, I. Kaminer, A. Shapira, M. Segev, and A. Arie, Phys. Rev. Lett. **108**, 113903 (2012).
[26] J. Broky, G. A. Siviloglou, A. Dogariu, and D. N. Christodoulides, Opt. Express **16**, 12880 (2008).
[27] R. Schley, I. Kaminer, E. Greenfield, R. Bekenstein, Y. Lumer, and M. Segev, Nat. Commun. **5**, 5189 (2014).
[28] M. A. Preciado, K. Dholakia, and M. Mazilu, Opt. Lett. **39**, 4950 (2014).
[29] N. Voloch-Bloch, Y. Lereah, Y. Lilach, A. Gover, and A. Arie, Nature (London) **494**, 331 (2013).
[30] N. K. Efremidis, V. Paltoglou, and W. von Klitzing, Phys. Rev. A **87**, 043637 (2013).
[31] I. Kaminer, J. Nemirovsky, M. Rechtsman, R. Bekenstein, and M. Segev, Nat. Phys. **11**, 261 (2015).
[32] J.-Y. Lu and J. F. Greenleaf, IEEE Trans. Ultrasonics, Ferroelectrics, Freq. Control **37**, 438 (1990).
[33] P. Zhang, T. Li, J. Zhu, X. Zhu, S. Yang, Y. Wang, X. Yin, and X. Zhang, Nat. Commun. **5**, 4316 (2014).
[34] Y. Li, C. Qiu, S. Xu, M. Ke, and Z. Liu, arXiv:1411.4776.
[35] J. N. Tjøtta and S. Tjøtta, J. Acoust. Soc. Am. **82**, 1429 (1987).
[36] J. N. Tjøtta and S. Tjøtta, J. Acoust. Soc. Am. **83**, 487 (1988).
[37] J. A. Ten Cate, Ph.D. thesis, The University of Texas at Austin, 1992.
[38] M. F. Hamilton and D. T. Blackstock, *Nonlinear Acoustics* (Academic, New York, 1998).
[39] O. V. Rudenko, Phys.-Usp. **49**, 69 (2006).
[40] Z. Lin, X. Guo, J. Tu, Q. Ma, J. Wu, and D. Zhang, J. Appl. Phys. **117**, 104503 (2015).
[41] A. D. Pierce, *Acoustics: An Introduction to Its Physical Principles and Applications* (Acoustical Society of America, Melville, NY,1989).
[42] D. M. Cottrell, J. A. Davis, and T. M. Hazard, Opt. Lett. **34**, 2634 (2009).
[43] E. Greenfield, J. Nemirovsky, R. El-Ganainy, D. N. Christodoulides, and M. Segev, Opt. Exp. **21**, 23785 (2013).
[44] S. Fu, Y. Tsur, J. Zhou, L. Shemer, and A. Arie, Phys. Rev. Lett. **115**, 034501 (2015).